Available online at www.sciencedirect.com
ScienceDirect
Ceramics International 35 (2009) 1625–1631
CERAMICS INTERNATIONAL
www.elsevier.com/locate/ceramint

Electrochemical properties of $LiNi_{1-y}Co_yO_2$ cathode materials synthesized from different starting materials by the solid-state reaction method

MyoungYoup Song [a,*], Jiunn Song [b], EuiYong Bang [a], Daniel R. Mumm [c]

[a] Division of Advanced Materials Engineering, Nanomaterials Processing Research Center, Engineering Research Institute, Chonbuk National University, 664-14 1ga Deogjindong Deogjingu Jeonju Jeonbuk, 561-756, Republic of Korea
[b] Fairmont Preparatory Academy, 2200 West Sequoia Avenue, Anaheim, CA 92801, USA
[c] Department of Chemical Engineering and Materials Science, University of California, Irvine, CA 92697-2575, USA

Received 23 May 2008; received in revised form 9 June 2008; accepted 13 September 2008
Available online 30 September 2008

Abstract

$LiNi_{1-y}Co_yO_2$ ($y = 0.1$, 0.3 and 0.5) were synthesized by the solid-state reaction method at 750 °C, 800 °C and 850 °C from $LiOH{\cdot}H_2O$, NiO and Co_3O_4 and from Li_2CO_3, NiO and Co_3O_4 as the starting materials. The physical and electrochemical properties of the synthesized $LiNi_{1-y}Co_yO_2$ were compared. The synthesized $LiNi_{1-y}Co_yO_2$ has the α-$NaFeO_2$ structure of the rhombohedral system (space group; $R\bar{3}m$). The particle size increases, on the whole, as the synthesis temperature increases or as the Co content increases. The particle sizes of the $LiNi_{1-y}Co_yO_2$ specimens synthesized from Li_2CO_3, NiO and Co_3O_4 at all three temperatures are larger than those of the specimens synthesized from $LiOH{\cdot}H_2O$, NiO and Co_3O_4 for all of the compositions. Among the samples synthesized from $LiOH{\cdot}H_2O$, NiO and Co_3O_4, $LiNi_{0.5}Co_{0.5}O_2$ synthesized at 800 °C has the largest first discharge capacity (174.3 mAh/g) and relatively good cycling performance. Among the samples synthesized from Li_2CO_3, NiO and Co_3O_4, $LiNi_{0.7}Co_{0.3}O_2$ synthesized at 750 °C has the best cycling performance (capacity fading rate 0.3 mAh/g cycle) and a relatively large first discharge capacity. The former has a larger value of I_{max}/B, a larger grain size and a smaller specific surface area than the latter.

Keywords: $LiNi_{1-y}Co_yO_2$; Solid-state reaction method; Different starting materials; Degree of displacement of the nickel and lithium ions; Discharge capacity; Capacity fading rate

1. Introduction

Lithium transition metal oxides such as $LiCoO_2$ [1,2], $LiNiO_2$ [3,4], $LiMnO_2$ [5] and $LiMn_2O_4$ [6,7] have been extensively investigated as cathode materials for rechargeable lithium batteries.

The Mn-containing lithium oxides, in which many researchers are interested, are $LiMnO_2$ and $LiMn_2O_4$, which have orthorhombic (*Pmnm*) and spinel (*Fd*3*m*) structures, respectively. Mn is cheaper than Co and Ni. $LiMnO_2$ is not easy to synthesize compared with $LiMn_2O_4$. However, $LiMnO_2$ has a theoretical charge–discharge capacity which is two times as high as that of $LiMn_2O_4$. Many researchers have studied Mn-containing lithium oxides, and found that their cycling performances are poor because Jahn-Teller distortion brings about the deterioration of the materials during charge–discharge [8].

The Co-containing lithium oxide, $LiCoO_2$, has been the most intensively studied for use in commercial rechargeable batteries, because of its large diffusivity and high operating voltage. However, it has the drawback that cobalt is expensive and toxic. It has a layered structure ($R\bar{3}m$).

The Ni-containing lithium oxide, $LiNiO_2$, with an $R\bar{3}m$ structure is considered to be a promising cathode material, due to its large discharge capacity and low cost. However, due to the size similarity of Li and Ni ($Li^+ = 0.72$ Å and $Ni^{2+} = 0.69$ Å), the $LiNiO_2$ is practically obtained in the non-stoichiometric composition, $Li_{1-y}Ni_{1+y}O_2$ [9,10], and the Ni^{2+} ions in the lithium planes obstruct the movement of the Li+ ions during charge and discharge [11,12].

A convenient way to overcome the drawbacks of $LiCoO_2$ and $LiNiO_2$ is to incorporate phases with the $LiNi_{1-y}Co_yO_2$ composition, because the presence of cobalt stabilizes the

* Corresponding author. Tel.: +82 63 270 2379; fax: +82 63 270 2386.
E-mail address: songmy@chonbuk.ac.kr (M. Song).

0272-8842/$34.00
doi:10.1016/j.ceramint.2008.09.003

structure in a strictly two-dimensional fashion, thus favoring good reversibility of the intercalation and deintercalation reactions [11,13–26]. Rougier et al. [11] reported that the stabilization of the two-dimensional character of the structure by cobalt substitution in $LiNiO_2$ is correlated with an increase in the cell performance, due to the decrease in the amount of extra-nickel ions in the inter-slab space which impede the lithium diffusion.

In our previous work [27], we studied the electrochemical properties of the cathode materials, $LiNi_{1-y}Co_yO_2$, synthesized from $LiOH{\cdot}H_2O$, Li_2CO_3, NiO, $NiCO_3$, Co_3O_4 and $CoCO_3$ by the solid-state reaction method. The cathode materials, $LiNi_{1-y}Co_yO_2$, synthesized from $LiOH{\cdot}H_2O$, NiO and Co_3O_4 and from Li_2CO_3, NiO and Co_3O_4 showed relatively good electrochemical properties.

In this work, $LiNi_{1-y}Co_yO_2$ ($y = 0.1$, 0.3 and 0.5) cathode materials were synthesized by the solid-state reaction method at different temperatures from $LiOH{\cdot}H_2O$, NiO and Co_3O_4 and from Li_2CO_3, NiO and Co_3O_4 as the starting materials. The physical and electrochemical properties of the synthesized samples were then compared.

2. Experimental

$LiOH{\cdot}H_2O$ (High Purity Chemical Laboratory Co., purity 99%), Li_2CO_3 (High Purity Chemical Laboratory Co., purity 99%), NiO (High Purity Chemical Laboratory Co., purity 99.9%) and Co_3O_4 (High Purity Chemical Laboratory Co., purity 99.9%) were used as the starting materials in order to synthesize $LiNi_{1-y}Co_yO_2$ by the solid-state reaction method.

The experimental procedure of this work is shown schematically in Fig. 1. The mixture of starting materials in the compositions $LiNi_{1-y}Co_yO_2$ ($y = 0.1$, 0.3 and 0.5) was mixed sufficiently and pelletized. This pellet was heat-treated in air at 650 °C for 20 h, and was then ground, mixed, pelletized again and calcined at 750 °C, 800 °C and 850 °C for 20 h. This pellet was cooled at a cooling rate of 50 °C/min, ground, mixed and pelletized again. It was then calcined again at 750 °C, 800 °C and 850 °C for 20 h.

The phase identification of the synthesized samples was carried out by X-ray diffraction (XRD) analysis with Cu K_α radiation using a Rigaku type III/A X-ray diffractometer. The scanning rate was 4°/min and the scanning range of the diffraction angle (2θ) was $10^\circ \leq 2\theta \leq 70^\circ$. The morphologies of the samples were observed using a field emission scanning electron microscope (FE-SEM). The particle size distributions and the specific surface areas of the samples were analyzed by a particle size analyzer (Malvern Instruments).

The electrochemical cells consisted of $LiNi_{1-y}Co_yO_2$ as a positive electrode, Li foil as a negative electrode, and an electrolyte [Purelyte (Samsung Chemicals Ltd.)] prepared by dissolving 1 M $LiPF_6$ in a 1:1(volume ratio) mixture of ethylene carbonate (EC) and dimethyl carbonate (DMC). A Whatman glass-fiber was used as the separator. To fabricate the positive electrode, 89 wt.% synthesized oxide, 10 wt.% acetylene black and 1 wt.% polytetrafluoroethylene (PTFE) binder were mixed in an agate mortar. The cell was assembled

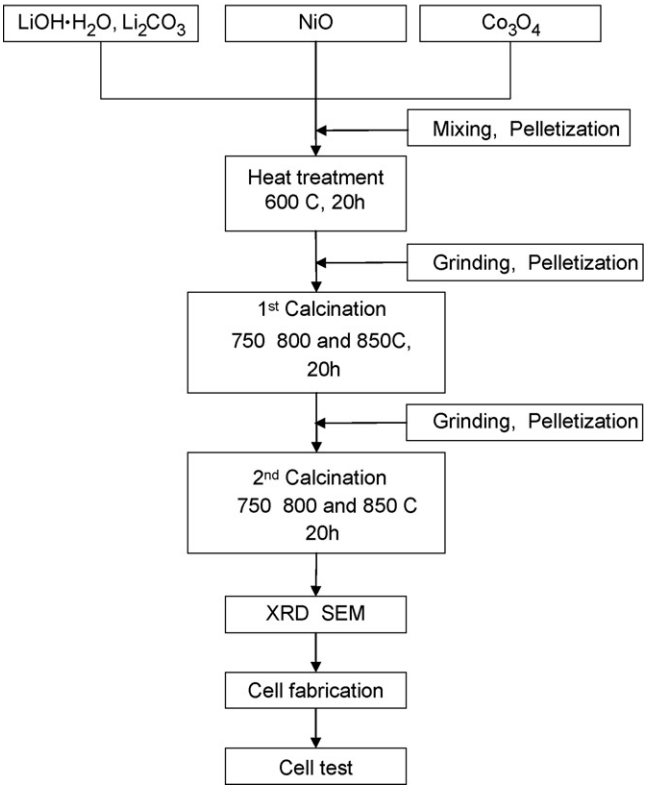

Fig. 1. Experimental procedure.

in a glove box filled with argon. All of the electrochemical tests were performed at room temperature with a potentiostatic/galvanostatic system. The cells were cycled at a current density of 200 μA/cm^2 between 3.2 V and 4.3 V.

3. Results and discussion

Fig. 2 shows the X-ray diffraction patterns of the $LiNi_{1-y}Co_yO_2$ ($y = 0.1$, 0.3 and 0.5) synthesized at 800 °C for 40 h from $LiOH{\cdot}H_2O$, NiO and Co_3O_4. They were identified

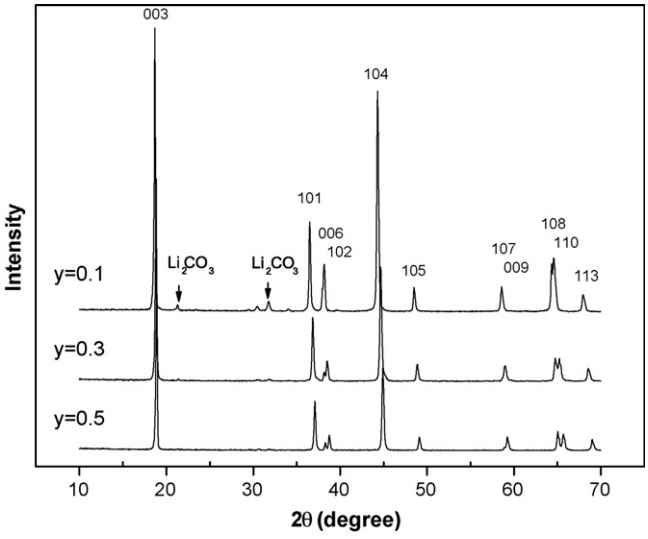

Fig. 2. XRD patterns of $LiNi_{1-y}Co_yO_2$ ($y = 0.1$, 0.3 and 0.5) powders synthesized at 800 °C for 40 h from $LiOH{\cdot}H_2O$, NiO and Co_3O_4.

Table 1
Intensity ratio, $I_{0\,0\,3}/I_{1\,0\,4}$, of 0 0 3 and 1 0 4 peaks for $LiNi_{1-y}Co_yO_2$ synthesized at 800 °C for 40 h from different starting materials.

Compositions	Starting materials	
	$LiOH{\cdot}H_2O$, NiO and Co_3O_4	Li_2CO_3, NiO and Co_3O_4
$y = 0.1$	0.928	0.962
$y = 0.3$	1.259	1.341
$y = 0.5$	1.477	1.410

as corresponding to the α-$NaFeO_2$ structure of the rhombohedral system (space group: $R\bar{3}m$). The diffraction angles of the peaks corresponding to this structure increase as the content of Co increases. Impurity peaks appear at the diffraction angles $2\theta = 21^\circ$ and 32°. These peaks were identified as those of the Li_2CO_3 phase. As the Co content increases, the intensities of these peaks decrease. The $LiNi_{1-y}Co_yO_2$ ($y = 0.1$, 0.3 and 0.5) synthesized at 750 °C and 850 °C from $LiOH{\cdot}H_2O$, NiO and Co_3O_4 showed X-ray diffraction patterns similar to those of the specimen synthesized at 800 °C. The X-ray diffraction patterns of $LiNi_{1-y}Co_yO_2$ ($y = 0.1$, 0.3 and 0.5) synthesized at 750 °C, 800 °C and 850 °C from Li_2CO_3, NiO and Co_3O_4 were similar to those of the specimens synthesized from $LiOH{\cdot}H_2O$, NiO and Co_3O_4.

Table 1 shows the intensity ratio, $I_{0\,0\,3}/I_{1\,0\,4}$, of the 0 0 3 and 1 0 4 peaks for $LiNi_{1-y}Co_yO_2$ synthesized at 800 °C for 40 h from the different starting materials. The intensity ratio, $I_{0\,0\,3}/I_{1\,0\,4}$, increases as the Co content increases. The 0 0 3 peak originates from the diffraction of only the $R\bar{3}m$ α-$NaFeO_2$ structure, while the 1 0 4 peak originates from the diffractions of both the $R\bar{3}m$ α-$NaFeO_2$ and $Fm\bar{3}m$ NaCl structures. Therefore, it is possible to calculate the fraction of each phase from the intensity ratio of the 0 0 3 and 1 0 4 peaks. Morales et al. [28] reported that the intensity ratio, $I_{0\,0\,3}/I_{1\,0\,4}$, of the completely stoichiometric composition $LiNiO_2$ is about 1.3. The $LiNi_{0.7}Co_{0.3}O_2$ specimens synthesized from the two different starting materials have $I_{0\,0\,3}/I_{1\,0\,4}$ values which are nearly 1.3. Ohzuku et al. [29] investigated the factors affecting the electrochemical reactivity of $LiNiO_2$. They reported that the intensity ratio of the 0 0 3 and 1 0 4 peaks is a key parameter of the degree of displacement of the nickel and lithium ions. As the intensity ratio of the 0 0 3 and 1 0 4 peaks increases, the degree of displacement of the nickel and lithium ions decreases. The disordered region prevents the extension and reduction of the interlayer distance between the NiO_2 sheets, making sliding between the basal planes impossible. Consequently, the nickel ions in the lithium sheet including the near neighbors are inactive for the electrochemical reaction. This is the reason that the samples having a high concentration of nickel ions at the lithium sites are inactive in nonaqueous lithium cells. Table 1 shows that the intensity ratio, $I_{0\,0\,3}/I_{1\,0\,4}$, increases as the Co content increases. This shows that the degree of displacement of the nickel and lithium ions decreases as the Co content increases. Ohzuku et al. [29] also reported that electroactive $LiNiO_2$ showed a clear split of the (1 0 8) and (1 1 0) lines, which appear in their XRD patterns at the diffraction angle near $2\theta = 65^\circ$ around [30]. Fig. 2 shows that the splitting of the (1 0 8) and (1 1 0) lines becomes clearer as the Co content increases.

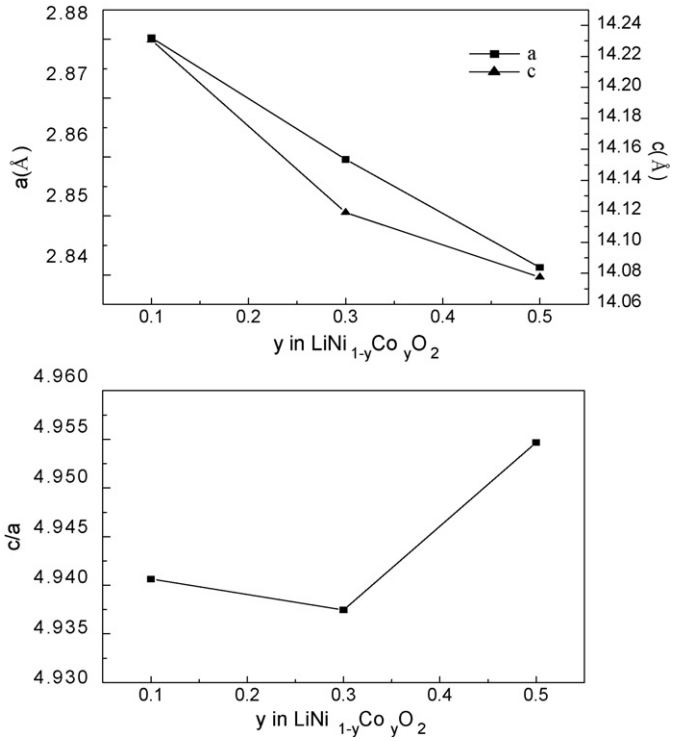

Fig. 3. Variation of lattice parameters, *a* and *c*, and their ratio, *c*/*a*, with y in $LiNi_{1-y}Co_yO_2$ synthesized at 800 °C from $LiOH{\cdot}H_2O$, NiO and Co_3O_4.

Fig. 3 shows the parameters of the hexagonal unit cell, *a* and *c*, and the degree of trigonal distortion, *c*/*a*, versus the Co content, *y*, in the $LiNi_{1-y}Co_yO_2$ synthesized at 800 °C from $LiOH{\cdot}H_2O$, NiO and Co_3O_4. As the Co content increases, the lattice parameters *a* and *c* decrease. The reason for this is that the radius of the Co ion [0.53 Å (low spin)] is smaller than that of the Ni ion [0.60 Å (low spin)]. The value of *c*/*a* decreases as *y* increases from 0.1 to 0.3 and then increases as *y* increases from 0.3 to 0.5. The increase in the value of *c*/*a* signifies the better development of the two-dimensional structure.

FE-SEM micrographs were obtained for the $LiNi_{1-y}Co_yO_2$ synthesized at 750 °C from $LiOH{\cdot}H_2O$, NiO and Co_3O_4. The particles are in the form of irregular polyhedrons, and large particles and small particles coexist. $LiNi_{0.7}Co_{0.3}O_2$ has the smallest particles and exhibits the smallest difference in particle size between the large particles and the small particles.

Fig. 4 shows the FE-SEM micrographs of the $LiNi_{1-y}Co_yO_2$ synthesized at 800 °C from $LiOH{\cdot}H_2O$, NiO and Co_3O_4. The particles are in the form of irregular polyhedrons and large particles and small particles coexist. $LiNi_{0.7}Co_{0.3}O_2$ has the smallest particles and $LiNi_{0.5}Co_{0.5}O_2$ has the largest particles.

FE-SEM micrographs were also obtained for the $LiNi_{1-y}Co_yO_2$ synthesized at 850 °C from $LiOH{\cdot}H_2O$, NiO and Co_3O_4. $LiNi_{0.9}Co_{0.1}O_2$ and $LiNi_{0.7}Co_{0.3}O_2$ are in the form of irregular polyhedrons and have large particles and small particles. $LiNi_{0.5}Co_{0.5}O_2$ has particles with round surfaces, while $LiNi_{0.7}Co_{0.3}O_2$ has the smallest particles.

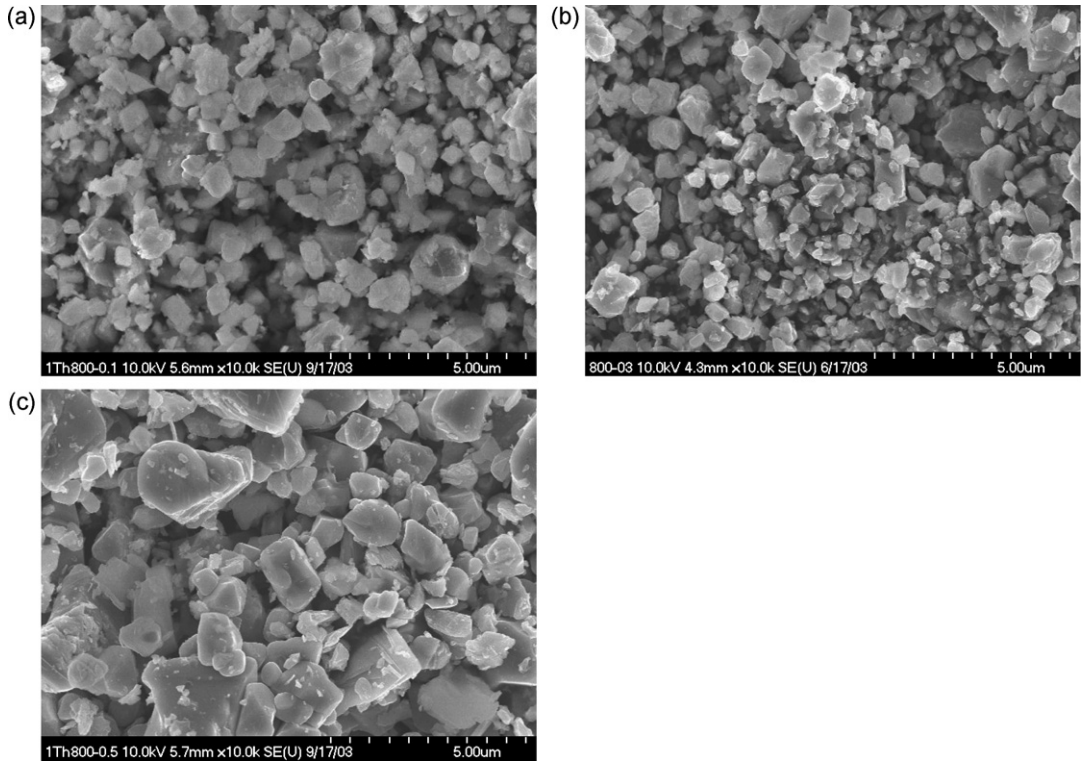

Fig. 4. FE-SEM micrographs of $LiNi_{1-y}Co_yO_2$ synthesized at 800 °C from $LiOH{\cdot}H_2O$, NiO and Co_3O_4; (a) $y = 0.1$, (b) $y = 0.3$ and (c) $y = 0.5$.

The FE-SEM micrographs of the $LiNi_{1-y}Co_yO_2$ synthesized at 750 °C, 800 °C (Fig. 4) and 850 °C show that the samples have small particles and large particles, and that $LiNi_{0.7}Co_{0.3}O_2$ has the smallest particles and the particle size increases as the synthesis temperature increases for the same composition.

Fig. 5 shows the FE-SEM micrographs of the $LiNi_{1-y}Co_yO_2$ synthesized at 750 °C from Li_2CO_3, NiO and Co_3O_4. These samples consist of small and large particles with irregular shapes and their clusters. As the value of y increases, the particle size becomes slightly larger. FE-SEM micrographs

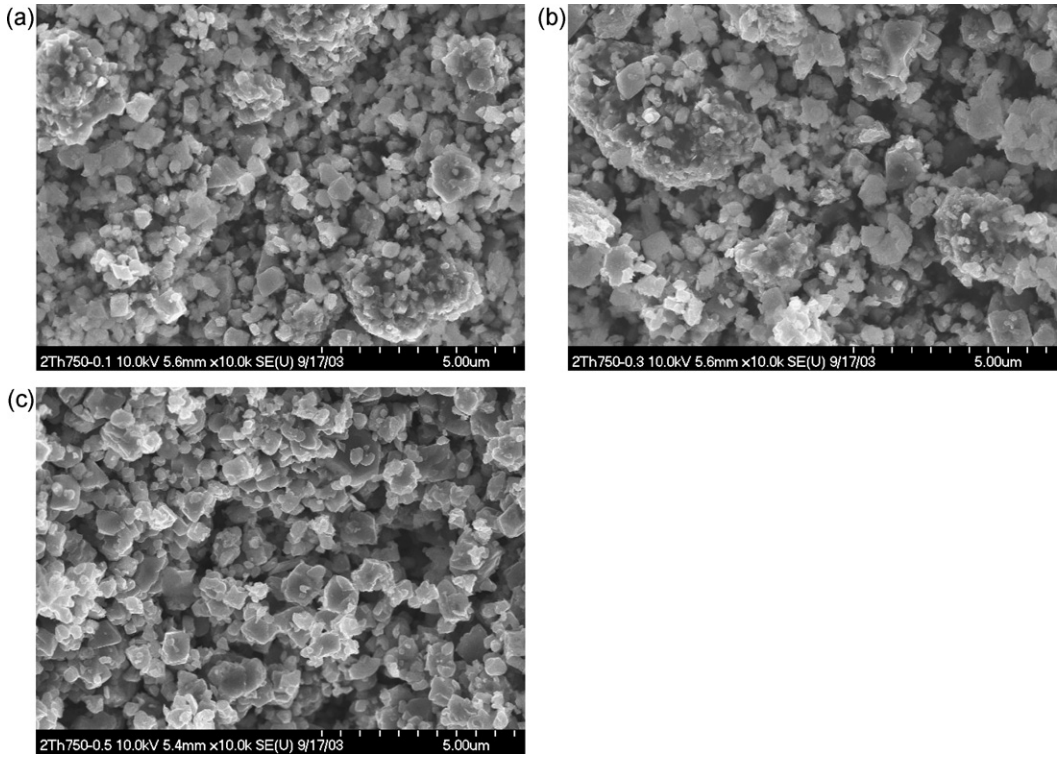

Fig. 5. FE-SEM micrographs of $LiNi_{1-y}Co_yO_2$ synthesized at 750 °C from Li_2CO_3, NiO and Co_3O_4; (a) $y = 0.1$, (b) $y = 0.3$ and (c) $y = 0.5$.

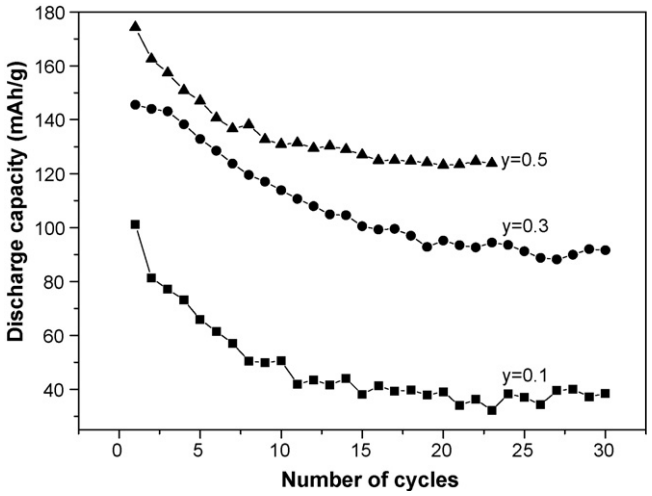

Fig. 6. Variations of discharge capacity at a current density of 200 μA/cm^2 with the number of cycles for $LiNi_{1-y}Co_yO_2$ synthesized at 800 °C for 40 h from $LiOH{\cdot}H_2O$, NiO and Co_3O_4.

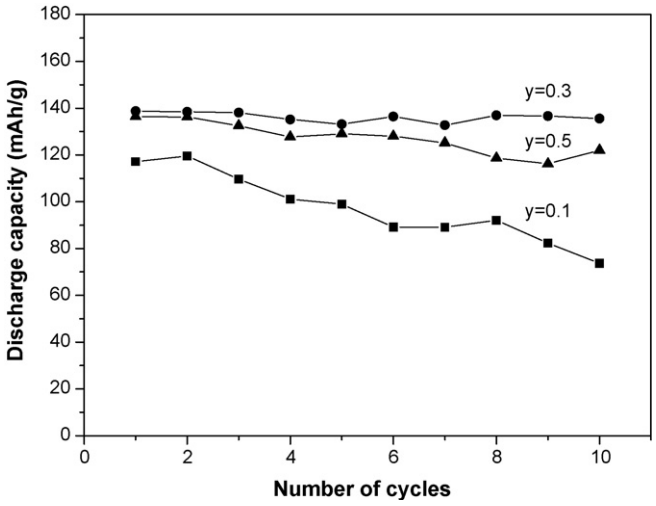

Fig. 7. Variations of discharge capacity at a current density of 200 μA/cm^2 with the number of cycles for $LiNi_{1-y}Co_yO_2$ synthesized at 750 °C for 40 h from Li_2CO_3, NiO and Co_3O_4.

were also obtained for the $LiNi_{1-y}Co_yO_2$ synthesized at 800 °C from Li_2CO_3, NiO and Co_3O_4. These samples consist of small and large particles in the form of irregular polyhedrons. The particles grow slightly larger as the content of Co increases.

FE-SEM micrographs were also obtained for the $LiNi_{1-y}Co_yO_2$ synthesized at 850 °C from Li_2CO_3, NiO and Co_3O_4. These specimens consist of small and large particles. The particle sizes are similar for all of the compositions, but $LiNi_{0.7}Co_{0.3}O_2$ has smaller particles compared with the other compositions. $LiNi_{0.5}Co_{0.5}O_2$ has particles with round surfaces.

From the FE-SEM micrographs of the $LiNi_{1-y}Co_yO_2$ synthesized at 750 °C (Fig. 5), 800 °C and 850 °C, we can observe that the samples have small particles and large particles, that the particle size generally increases as the content of Co increases at the same synthesis temperature, and that the particle size generally increases as the synthesis temperature increases at the same composition.

Fig. 6 shows the variations of the discharge capacity at a current density of 200 μA/cm^2 with the number of cycles (n) for the $LiNi_{1-y}Co_yO_2$ synthesized at 800 °C from $LiOH{\cdot}H_2O$, NiO and Co_3O_4. $LiNi_{0.5}Co_{0.5}O_2$ has the largest first discharge capacity (174.3 mAh/g), followed in order by $LiNi_{0.7}Co_{0.3}O_2$ (145.5 mAh/g) and $LiNi_{0.9}Co_{0.1}O_2$. $LiNi_{0.5}Co_{0.5}O_2$ has a relatively good cycling performance with a discharge capacity of 123.8 mAh/g at the 23rd cycle. Its capacity fading rate is 1.83 mAh/g cycle. The $LiNi_{1-y}Co_yO_2$ specimen synthesized at 800 °C had a larger first discharge capacity and better cycling performance than those synthesized at 750 °C and 850 °C.

Fig. 7 shows the variations of the discharge capacity at a current density of 200 μA/cm^2 with the number of cycles (n) for the $LiNi_{1-y}Co_yO_2$ synthesized at 750 °C from Li_2CO_3, NiO and Co_3O_4. The samples with $y = 0.3$ and $y = 0.1$ have the largest (138.8 mAh/g) and smallest first discharge capacities, respectively. The sample with $y = 0.3$ exhibits excellent cycling performance with a discharge capacity of 135.6 mAh/g at $n = 10$. Its capacity fading rate is 0.3 mAh/g cycle. The sample with $y = 0.5$ exhibits relatively good cycling performance. $LiNi_{0.7}Co_{0.3}O_2$ synthesized at 800 °C had a first discharge capacity of 153.8 mAh/g, but its cycling performance was poor. $LiNi_{1-y}Co_yO_2$ synthesized at 850 °C from Li_2CO_3, NiO and Co_3O_4 showed worse electrochemical properties than these samples.

Table 2 shows the values of *c*/*a*, the unit cell volumes, the values of I_{max}/B, the grain sizes, mean particle sizes, specific surface areas, first discharge capacities and capacity fading

Table 2
Physical and electrochemical properties of $LiNi_{1-y}Co_yO_2$ synthesized at various temperatures from $LiOH{\cdot}H_2O$, NiO and Co_3O_4.

Synthesis temp. (°C)	Composition	*c*/*a*	Unit cell volume (Å^3)	(I_{max}/B) $\times 10^{-6}$	Grain size (Å)	Mean particle size (μm)	Specific surface area (m^2/g)	First discharge cpapcity (mAh/g)	Capacity fading rate (mAh/g cycle)
750	$LiNi_{0.9}Co_{0.1}O_2$	4.921	101.306	1.504	387.1	5.91	1.76	131.8	6.5
750	$LiNi_{0.7}Co_{0.3}O_2$	4.963	100.408	1.193	449.8	20.56	1.09	80.9	3.6
750	$LiNi_{0.5}Co_{0.5}O_2$	4.966	99.374	0.850	423.8	12.12	1.29	66.1	2.7
800	$LiNi_{0.9}Co_{0.1}O_2$	4.941	102.238	6.331	470.8	15.11	1.48	101.2	5.2
800	$LiNi_{0.7}Co_{0.3}O_2$	4.937	99.986	4.110	428.3	20.16	0.95	145.5	3.9
800	$LiNi_{0.5}Co_{0.5}O_2$	4.955	98.416	3.620	452.4	33.08	0.81	174.3	4.5
850	$LiNi_{0.9}Co_{0.1}O_2$	4.923	101.306	5.600	435.3	21.72	1.08	113.3	6.1
850	$LiNi_{0.7}Co_{0.3}O_2$	4.956	100.065	5.300	470.9	11.64	1.18	146.2	6.3
850	$LiNi_{0.5}Co_{0.5}O_2$	4.959	98.476	6.826	500.2	7.23	1.47	134.4	8.0

Table 3
Physical and electrochemical properties of $LiNi_{1-y}Co_yO_2$ synthesized at various temperatures from Li_2CO_3, NiO and Co_3O_4.

Synthesis temperature (°C)	Composition	*c*/*a*	Unit cell volume (Å^3)	(I_{max}/*B*) $\times 10^{-6}$	Grain size (Å)	Mean particle size (μm)	Specific surface area (m^2/g)	First discharge cpapcity (mAh/g)	Capacity fading rate (mAh/g cycle)
750	$LiNi_{0.9}Co_{0.1}O_2$	4.933	101.682	3.648	361.1	13.95	1.39	117.2	4.8
750	$LiNi_{0.7}Co_{0.3}O_2$	4.936	100.045	2.522	334.1	18.25	1.26	138.8	0.3
750	$LiNi_{0.5}Co_{0.5}O_2$	4.942	99.721	1.244	287.6	20.13	1.15	136.5	2.1
800	$LiNi_{0.9}Co_{0.1}O_2$	4.920	101.291	4.126	372.8	21.05	1.31	122.1	3.9
800	$LiNi_{0.7}Co_{0.3}O_2$	4.950	100.034	3.484	383.4	13.05	1.67	153.8	7.3
800	$LiNi_{0.5}Co_{0.5}O_2$	4.965	98.771	2.387	385.3	20.74	1.31	147.6	1.6
850	$LiNi_{0.9}Co_{0.1}O_2$	4.936	101.637	5.236	398.6	24.69	1.41	119.5	4.8
850	$LiNi_{0.7}Co_{0.3}O_2$	4.929	99.365	4.031	392.8	19.06	1.40	109.0	8.7
850	$LiNi_{0.5}Co_{0.5}O_2$	4.956	98.460	2.804	402.7	24.36	1.08	149.2	5.9

rates of $LiNi_{1-y}Co_yO_2$ synthesized at various temperatures from $LiOH{\cdot}H_2O$, NiO and Co_3O_4.

Dahn et al. [31] defined the intensity ratio, *R,* as the relative intensity of the (1 0 2, 0 0 6) Bragg peak near $2\theta = 38^\circ$ as compared with that of the (1 0 1) peak near $2\theta = 36.5^\circ$. Their results showed that the intensity ratio, *R*, increases as the unit cell volume increases. They also showed that the intensity ratio, *R*, increases rapidly as *x* decreases in $Li_xNi_{2-x}O_2$. This suggests that, as the unit cell volume increases, *x* decreases in $Li_xNi_{2-x}O_2$. $Li_xNi_{2-x}O_2$ can be expressed as $(Li_xNi_{1-x})NiO_2$. A decrease in *x* in $Li_xNi_{2-x}O_2$ corresponds to an increase in the degree of displacement of the nickel and lithium ions. We introduced an index to investigate the crystallinity of the samples. The crystallinity is proportional to the sharpness of the diffraction peak of the XRD powder patterns. We can numerate the sharpness by examining the value of I_{max}/B, where I_{max} is the maximum intensity of the diffraction peak and *B* is the width of the peak at an intensity equal to half I_{max}. We named I_{max}/B the ''crystallinity index [32]''. To obtain the grain size, *t*, we used the Scherrer formula:

$$t = \frac{0.9\lambda}{B\cos\theta_B} \quad (1)$$

where λ is the wavelength of the X-ray used, *B* is the width of the diffraction peak considered at an intensity equal to half I_{max}, and θ_B is the Bragg angle of the diffraction peak [33]. The capacity fading rates were obtained by the least squares method using the discharge capacities between the first cycle and the tenth cycle. The values of *c*/*a* were in the range of 4.921–4.966. The unit cell volumes were 98.416–102.238 Å^3. The unit cell volumes of the samples calcined at the same temperature decrease as the Co content increases, indicating that the degree of displacement of the nickel and lithium ions decreases as the Co content increases. The values of I_{max}/B were in the range of 0.850×10^6 to 6.826×10^6. The grain sizes were 387.1–500.2 Å. The mean particle sizes were 5.91–33.08 μm. The specific surface areas were 0.81–1.76 m^2/g. The first discharge capacities were 66.1–174.3 mAh/g. The capacity fading rates were 2.7–8.0 mAh/g cycle. $LiNi_{0.5}Co_{0.5}O_2$ synthesized at 800 °C, which has the largest first discharge capacity and relatively good cycling performance, has a relatively large value of *c*/*a*, a relatively large grain size and the smallest specific surface area.

Table 3 shows the values of *c*/*a*, the unit cell volumes, the values of I_{max}/B, the grain sizes, mean particle sizes, specific surface areas, first discharge capacities and capacity fading rates of $LiNi_{1-y}Co_yO_2$ synthesized at various temperatures from Li_2CO_3, NiO and Co_3O_4. The values of *c*/*a* were in the range of 4.920–4.965. The unit cell volumes were 98.460–101.682 Å^3. The unit cell volumes of the samples calcined at the same temperature decrease as the Co content increases, indicating that the degree of displacement of the nickel and lithium ions decreases as the Co content increases. The values of I_{max}/B were in the range of 1.244×10^6 to 5.236×10^6. The grain sizes were 287.6–402.7 Å. The mean particle sizes were 13.05–24.69 μm. The specific surface areas were 1.08–1.67 m^2/g. The first discharge capacities were 109.0–153.8 mAh/g. The capacity fading rates were 0.3–8.7 mAh/g cycle. $LiNi_{0.7}Co_{0.3}O_2$ synthesized at 750 °C, which has the smallest capacity fading rate and a relatively large first discharge capacity, has a relatively small grain size and relatively small specific surface area. $LiNi_{0.5}Co_{0.5}O_2$ synthesized at 800 °C from $LiOH{\cdot}H_2O$, NiO and Co_3O_4 has a larger value of I_{max}/B, a larger grain size and a smaller specific surface area compared with $LiNi_{0.7}Co_{0.3}O_2$ synthesized at 750 °C from Li_2CO_3, NiO and Co_3O_4.

4. Conclusions

$LiNi_{1-y}Co_yO_2$ ($y = 0.1$, 0.3 and 0.5) were synthesized by the solid-state reaction method at 750 °C, 800 °C and 850 °C from $LiOH{\cdot}H_2O$, NiO and Co_3O_4 and from Li_2CO_3, NiO and Co_3O_4. $LiNi_{1-y}Co_yO_2$ has the α-$NaFeO_2$ structure of the rhombohedral system (space group; $R\bar{3}m$). The particle size increases, on the whole, as the synthesis temperature increases or as the Co content increases. The particle sizes of the $LiNi_{1-y}Co_yO_2$ specimens synthesized at all three temperatures from Li_2CO_3, NiO and Co_3O_4 are larger than those of the specimens synthesized from $LiOH{\cdot}H_2O$, NiO and Co_3O_4 for all of the compositions. Among the samples synthesized from $LiOH{\cdot}H_2O$, NiO and Co_3O_4, $LiNi_{0.5}Co_{0.5}O_2$ synthesized at 800 °C has the largest first discharge capacity (174.3 mAh/g) and relatively good cycling performance. Among the samples synthesized from Li_2CO_3, NiO and Co_3O_4, $LiNi_{0.7}Co_{0.3}O_2$ synthesized at 750 °C has the best cycling performance (capacity fading rate 0.3 mAh/g cycle) and a relatively large

first discharge capacity. The intensity ratio, $I_{0\,0\,3}/I_{1\,0\,4}$, increases as the Co content increases. The unit cell volumes of the samples calcined at the same temperature decrease as the Co content increases. These two results indicate that the degree of displacement of the nickel and lithium ions decreases as the Co content increases.

References

[1] K. Ozawa, Solid-State Ionics 69 (1994) 212.
[2] Z.S. Peng, C.R. Wan, C.Y. Jiang, J. Power Sources 72 (1998) 215.
[3] J.R. Dahn, U. von Sacken, M.W. Juzkow, H. Al-Janaby, J. Electrochem. Soc. 138 (1991) 2207.
[4] M.Y. Song, R. Lee, Solid-State Ionics 111 (2002) 97.
[5] A.R. Armstrong, P.G. Bruce, Nature 381 (1996) 499.
[6] J.M. Tarascon, E. Wang, F.K. Shokoohi, W.R. Mckinnon, S. Colson, J. Electrochem. Soc. 138 (1991) 2859.
[7] M.Y. Song, D.S. Ahn, Solid-State Ionics 112 (1998) 245.
[8] M.M. Thackeray, A. de Kock, M.H. Rossouw, D. Liles, R. Bittihn, D. Hoge, J. Electrochem. Soc. 139 (1992) 363.
[9] P. Barboux, J.M. Tarascon, F.K. Shokoohi, J. Solid State. Chem. 94 (1991) 185.
[10] J. Morales, C. Perez-Vicente, J.L. Tirado, Mater. Res. Bull. 25 (1990) 623.
[11] A. Rougier, I. Saadoune, P. Gravereau, P. Willmann, C. Delmas, Solid-State Ionics 90 (1996) 83.
[12] B.J. Neudecker, R.A. Zuhr, B.S. Kwak, J.B. Bates, J. Electrochem. Soc. 145 (1998) 4161.
[13] C. Delmas, I. Saadoune, Solid-State Ionics 53–56 (1992) 370.
[14] E. Zhecheva, R. Stoyanova, Solid-State Ionics 66 (1993) 143.
[15] C. Delmas, I. Saadoune, A. Rougier, J. Power Sources 43–44 (1993) 595.
[16] A. Ueda, T Ohzuku, J. Electrochem. Soc. 141 (1994) 2010.
[17] M. Menetrier, A. Rougier, C. Delmas, Solid State Commun. 90 (1994) 439.
[18] R. Alcantara, J. Morales, J.L. Tirado, J. Electrochem. Soc. 142 (1995) 3997.
[19] B. Banov, J. Bourilkov, M. Mladenov, J. Power Sources 54 (1995) 268.
[20] Y.M. Choi, S.I. Pyun, S.I. Moon, Solid-State Ionics 89 (1996) 43.
[21] S.J. Lee, J.K. Lee, D.W. Kim, H.K. Baik, J. Electrochem. Soc. 143 (1996) L268.
[22] D. Caurant, N. Baffier, B. Garcia, J.P. Pereira-Ramos, Solid State Ionics 91 (1996) 45.
[23] K. Amine, H. Yasuda, Y. Fujita, Ann. Chim. Sci. Mater. 23 (1998) 37.
[24] C.C. Chang, N. Scarr, P.N. Kumta, Solid-State Ionics 112 (1998) 329.
[25] K. Kubo, S. Arai, S. Yamada, M. Kanda, J. Power Sources 81–82 (1999) 599.
[26] E. Levi, M.D. Levi, G. Salitra, D. Aurbach, R. Oesten, U. Heider, L. Heider, Solid-State Ionics 126 (1999) 97.
[27] M.Y. Song, H. Rim, E.Y. Bang, J. Appl. Electrochem. 34 (2004) 383.
[28] J. Morales, C. Pérez-Vicente, J.L. Tirado, Mater. Res. Bull. 25 (1990) 623.
[29] T. Ohzuku, A. Ueda, M. Nagayama, J. Electrochem. Soc. 140 (1993) 1862.
[30] T. Ohzuku, H. Komori, K. Sawai, T. Hirai, Chem. Express. 5 (1990) 733.
[31] J.R. Dahn, U. von Sacken, C.A. Michal, Solid State Ionics 44 (1990) 87.
[32] D.S. Ahn, M.Y. Song, J. Electrochem. Soc. 147 (2000) 874.
[33] H.P. Klug, L.E. Alexander, X-ray Diffraction Procedures for Polycrystalline and Amorphous Materials. A Wiley-Interscience Publication, John Wiley, New York, 1974, pp. 656–657.